Factors influencing surface morphology of anodized TiO_2 nanotubes

D. Regonini[1], A. Satka[2], A. Jaroenworaluck[3], D.W.E. Allsopp[4], C. R. Bowen[1] and R. Stevens[1]

[1]*Materials Research Centre, Department of Mechanical Engineering, University of Bath (UK)*
[2] *Faculty of Electrical Engineering and Information Technology STU and International Laser Center, Bratislava, Slovakia; Department of Microelectronics, Slovak University*
[3]*National Metal and Materials Technology Center, 114, Thailand Science Park, Paholyothin Road, Klong 1, Klong Luang, Pathumthani 12120, Thailand*
[4]*Department of Electronics and Electrical Engineering, University of Bath (UK)*

Corresponding author: D. Regonini,
email address: d.regonini@hotmail.com

Abstract

This paper investigates the formation mechanism of ribs on the outer wall of anodized TiO_2 nanotubes (NTs) prepared in a NaF/Glycerol electrolyte containing 2wt% of water. The effect of potential and time on the morphology of the NTs is evaluated along with growth efficiency (% of total charge at the electrode used to form the oxide) and X-ray Photoelectron Spectroscopy (XPS) measurements, providing an insight into the mechanism of formation of ribs. XPS analysis confirms the presence of fluorine, as TiF_6^{2-} , and carbon as impurities in the anodic film. The growth efficiency of the process decreases from ~70% at 10V to 55-58% at 20-30V and 14% at 40V. Similarly, the anodic growth factor (migration of ions expressed as the maximum radius of the "oxide cell" per applied potential, nm V^{-1}) decreases at higher potentials, due to oxygen bubbles evolving at the anode at 20-40V and disrupting the anodizing process. The formation of gas bubbles also affects the morphology of the NTs; while NTs are smooth at 10V, oxide rings appear over the range 20-40V. Partial dissolution of the oxide rings due to fluorine ions eventually re-shapes the NTs forming ribs, whereas excessive dissolution over extended anodizing times tends to smoothen the NTs and eventually leads to collapse of the NTs. On the basis of these observations, we suggest oxygen evolution (requiring a minimum amount of water in the electrolyte and a sufficiently high potential 20-40V) plays a primary role on the formation of ribs on anodized TiO_2 NTs. Ribs are also observed on NTs grown in aqueous electrolytes, although since dissolution is more difficult to control the resulting structure is more irregular than in organic media.

Keywords: TiO_2, nanotubes, anodization, organic electrolytes, fluorine ions

1. Introduction

Since the first reports in 1999-2001[1-3], the synthesis of anodized self-organized titanium dioxide nanotubes (TiO_2 NTs) and their use in photo-catalysis, solar cells, biomedicine and sensing has been widely investigated [4]. The growth of anodized TiO_2 NTs is usually accomplished using fluorine containing aqueous [5] or organic [6] electrolytes. Until recently, the accepted growth mechanism was based on Field-Enhanced Oxide Dissolution (FAD) at the pore/tube base which is balanced with oxide formation at the Metal/ Metal Oxide (M/MO) interface. This balance ensures continuous anodization and growth of pores/tubes which leads to the formation of porous anodic aluminium oxide (AAO) [7] and anodic TiO_2 NTs [8]. However, an alternative mechanism has been proposed, that of a field-assisted 'plastic flow' model, where the barrier oxide at the M/MO interface is constantly displaced upwards to form the pore/tube walls for AAO[9, 10], TiO_2 NTs [11] and other anodized self-organized (valve) metal oxides [4]. The 'plastic flow' mechanism is supported by experimental evidence involving the use of tracers to evaluate the movement of species within the anodic film. The displacement of material is a response to the stress generated by electrostriction [12] as a result of the high applied electric field, 10^6-10^8 V cm^{-1} [13] and the volume expansion associated with oxidation process [14, 15]. Several studies [16-18] have reported some form of visco-plastic deformation of the anodic film, an important requirement to ensure outward displacement of the

oxide. This ability to deform is also inferred from the behaviour of gas bubbles trapped within anodic alumina, which can expand without rupturing the film [19, 20].

One fascinating feature of TiO_2 NTs is the morphology of their outer wall. The amount of water in the electrolyte is a crucial factor that determines whether the NTs are smooth or exhibit a 'ribbed' appearance [21]. Ribs (also called ripples) are always observed in NTs grown in aqueous electrolyte, whereas NTs prepared in organic media can be either smooth or have ribs depending on whether the water content is below or above a critical amount (typically in the order of few wt%). Macak et al. [22] suggested that ribs formed by an aqueous electrolyte are a result of current oscillations due to periodic pH bursts at the nanotube base. Recently, Berger et al. [23] provided evidence of the existence of a fluorine rich layer at the triple points between TiO_2 NTs pore cells, supporting our earlier observations [24]. Assuming dissolution is accelerated by the higher fluorine content, this layer is thought to be responsible for the transition from TiO_2 nanopores to nanotubes in organic electrolytes [25, 26]. The formation of ribs would then occur intermittently as a consequence of the fluorine rich electrolyte penetrating between NTs, partially dissolving the oxide and creating a sufficiently high electric field for ion migration and the formation of an anodic film around the external NTs walls [27]. This model implies the formation of ribs at the Metal Oxide (MO)/Electrolyte interface, whereas it has been suggested that no material is grown away from the M/MO interface and Ti ions reaching the MO/electrolyte interface are directly ejected into the solution [9-11].

The objective of this paper is to examine in detail the mechanism of formation of ribs and propose a model which holds true for both aqueous and organic electrolytes. To gain an insight on the process, we consider how the anodizing potential, time and dissolution affect the morphology of the NTs and the ribs on their surface.

2. Materials and Experimental Method

A commercially pure (99.6%) titanium sheet (0.5mm thick) was used as anode, with a platinum mesh acting as the cathode. Prior to anodizing, Ti specimens were ultrasonically cleaned in isopropyl alcohol. The electrolyte consisted of an organic glycerol based solution containing 2wt% water and 0.5wt% of sodium fluoride (NaF). The electrolyte's pH and dynamic viscosity prior to anodization were 6.8 and 0.5 Pa s respectively at 20°C. Anodizing was performed by applying an initial potential ramp of 100mV s^{-1} before holding the potential constant within the range 10-40V, while the electrolyte was slightly stirred. Anodizing times up to 20h were investigated. For comparison, a specimen was anodized at 25V in an aqueous based 1M Na_2SO_4, 0.5wt% NaF solution (pH ~7) solution. Specimens were examined using a Scanning Electron Microscope (SEM), (JEOL JSM6480LV), and a Field Emission SEM (FE SEM LEO 1550 with in-lens secondary electron detector) for higher resolution images. A 300x700μm^2 specimen area was employed during surface analysis and a 110µm circular spot during depth profiling. The conditions used for XPS investigations are available elsewhere [28]. Data were processed using a Computer-Aided-Software-Analysis (CASA XPS), with semi-quantitative data obtained by applying a Shirley algorithm to remove spectra background and obtain Gaussian/Lorentzian product functions, to fit multi-component peaks [29].

3. Result and Discussion

3.1 XPS analysis

The XPS analysis in **Fig. 1** shows the composition of a typical specimen anodized in a NaF/Glycerol electrolyte, with the main impurities being fluorine ions and carbon species. The high carbon content is related to contamination from both the electrolyte and the atmosphere, the latter can contribute up to 10-20at% on TiO_2 surfaces [30]. The rate of growth of the anodic oxide in glycerol is far slower than in water based electrolytes [31] and this is reflected in the slower development of the O1s peak, **Fig.2a-c**, which makes it possible to monitor the progress of the anodizing process. After anodizing for 10 minutes, **Fig. 2a**, the oxygen signal is dominated by organic species (533.4eV) and OH^- species (532eV), the majority of which are of organic nature (C-OH groups); although the broad OH peak suggests the NTs to be effectively hydrated when grown in glycerol. After 10 minutes, **Fig. 2a**, the oxide component (530.7eV) accounts for only 16.7at% of the total oxygen signal. The oxide signal becomes dominant after 60 minutes, **Fig. 2b**, and depth profiling, **Fig. 2c,** indicates that contributions due to organic species is limited to the outer layers of the anodic film, with the oxide component accounting for at least 60at% of the total O1s signal. XPS analysis of

the F1s peak is important in the context of this work since it quantifies the contamination of the oxide with fluorine, which is responsible for the time dependent dissolution and morphology of the anodic film and will be discussed later. The fluorine impurity content, **Fig. 2d**, primarily in the form of $[TiF_6]^{2-}$ at 684.9eV, is ~8at%, twice as much as that measured in aqueous media[28]; this is not surprising considering the high viscosity of glycerol, compared to an aqueous media, which limits ion diffusion and the lower solubility of fluorine species in organic solutions. Since the measurement area in XPS is of the order of hundreds of μm^2, the fluorine concentration across the anodic film on the macro-scale is relatively homogeneous, as confirmed by the depth profiling analysis in **Fig. 2d,** which shows no significant changes in the concentration measured before and after 180s etching of the film. It is well known that the fluorine content can be drastically reduced by annealing (below 1at% at 400ºC) [28] and that it is inhomogenously distributed on the nanoscale. Fluorine tends to concentrate on the outer wall of the NT and incorporated in an amorphous layer; it is present up to 500-600ºC, facilitating liquid phase sintering and collapse of the NTs during annealing [24].

3.2 Effect of Anodizing Potential on Nanotube Morphology

Table 1 summarises the main parameters of the NTs grown, such as internal (d_i) and external (d_e) diameters, wall thickness **(**w**)** and anodic growth factor (f_g). The d_i and d_e values are consistent with previous work [32] and both increase with increasing potential, being 19.5nm and 40.9nm respectively at 10V and 75.9nm and 124.2nm at 40V. By plotting d_i and d_e against potential, **Fig. 3**, a quasi-linear relationship is observed, in agreement with literature for similar potential ranges [33]. The anodic growth factor, f_g, measured in nm V^{-1}, expresses the migration of ions within the anodic film and from Yasuda's model [34] is related to d_e in the form $d_e = 2Vf_g$, where V is the anodizing potential. The anodizing potential determines the migration of ions and the maximum radius ($d_e/2$) of an "oxide cell". The value of d_e is determined from SEM observations and chemical dissolution is often inhomogeneous throughout the NTs layer, hence f_g values in **Table 1** are indicative values only. It is apparent that f_g decreases from 2.0nm V^{-1} at 10V to 1.5-1.7nm V^{-1} when the anodizing potential is increased to 20-40V. A factor leading to a decrease of f_g with increasing potential is the higher chemical dissolution occurring at higher potential, with a higher electric field weakening the Ti-O bond and favouring the chemical attack of fluorine ions. Evolution of oxygen at the anode is also contributing to the reduction of f_g. While no oxygen evolution is observed at 10V, we observe gas bubbles at the anode within the potential range 20-40V; this indicates that above 20V oxygen ions are not solely contributing to the formation of any oxide, but some are instead discharged, generating an electronic current. Furthermore gas bubbles are an obstacle to ionic migration and f_g is therefore lower at 20-40V than at 10V. As will be discussed later, SEM analysis indicates that the applied potential and the formation of oxygen bubbles at the anode are also affecting the morphology of the NTs.

3.3. Growth Efficiency

Further information on the anodizing process as a function of anodization conditions is gained by investigating its efficiency for a given anodizing potential. If we assume that all the anodization charge is used to form the anodic structure, it is possible to estimate an ideal thickness, $T_{id.}$, against which we compare the measured thickness, T_{real}, obtained from SEM observations. From Faraday's law:

$$T_{id.} = \frac{QM_w}{AencN_A\rho} \cdot 10^7 \quad \text{(eq. 1)}$$

where $T_{id.}$ is expressed in nm, Q is the electric charge (A sec), M_w the molecular weight of TiO_2 (79.9 g mol^{-1}), A is the surface area (0.8cm^2), e is the charge on an electron ($1.602 \cdot 10^{-19}$ A sec), n is the number of electrons involved per Ti atom (taken as four, assuming complete oxidation), c is the number of Ti atom per

TiO_2 molecule (1), N_A is Avogadro's constant (mol^{-1}) and ρ is the density of amorphous TiO_2 (3.1g cm^{-3}) [35]. The ratio $T_{real}/T_{id.}$ provides a measure of the growth efficiency (ε_{NTs}) of the process. If it is assumed that the growth mechanism occurs mainly by the 'plastic flow' mechanism rather than field assisted dissolution, the porosity of the film, P, should be taken into account since $T_{id.}$ is calculated for a non-porous film and would have a smaller thickness compared to a porous layer with the same volume of oxide. For a 'plastic flow' model the effect of dissolution is considered secondary in the formation of porosity since NTs are generated in response to a mechanical stress induced by volume expansion and electrostriction. Experimental evidence reveal that the NTs grow much larger than expected for a purely field assisted dissolution mechanism, with an expansion factor (as a result of the metal converting into an oxide) up to 3, whereas the expansion factor (Pilling-Bedworth ratio) of amorphousTiO_2 is ~2.43 [4]. The porosity P of a hexagonally self-organized the NTs array can be calculated as follows [36]:

$$P = 1 - \left[\frac{2\pi}{\sqrt{3}} \cdot \frac{(d_i w + w^2)}{l^2} \right] \qquad \text{(eq. 2)}$$

where d_i is the inner diameter of the NTs, w is the wall thickness, and l is the centre to centre distance between NTs. Considering that when grown in organic media, the NTs originate from hexagonally ordered nanopores due to preferential etching at fluorine rich boundaries (triple points) [23] and the gaps between NTs can be ignored (as they are originally filled with oxide), hence $l = d_e = 2w + d_i$. The revised efficiency accounting porosity is therefore given by:

$$\varepsilon_{NTs} = \frac{T_{real}}{T_{id.}} \cdot (1 - P) \qquad \text{(eq. 3)}$$

The efficiency was calculated using the total charge passed over the first 4h of the anodizing process, since dissolution has a considerable effect on NTs length for longer anodization times [32]. **Table 2** summarises the results; the efficiency values in parenthesis do not take into account the porosity of the film and this explains some anomalous efficiencies that exceed 100%. The corrected values that account for porosity provide a more realistic overview. ε_{NTs} decreases with increasing potential, from 71% at 10V, to 55-58% at 20-30V and finally 14% at 40V. The drop in efficiency observed at 40V is due to evolution of oxygen bubbles at the anode becoming more significant than at 20-30V, with a greater portion of oxygen ions being discharged rather than contributing to the formation of anodic oxide. Several reasons need to be taken into account to explain the efficiency losses observed during the formation of the NTs, which grow by an ionic driven process. Some of the Ti ions are directly ejected into the electrolyte without forming any oxide [9-11]. Dissolution, although secondary, may thin away the oxide layer or detach of a section of the film and finally there may be "electronic" side reactions occurring at the anode such as oxygen evolution, which we observe for specimens anodized over the range 20-40V. As previously discussed gas bubbles are associated with a decrease of f_g and, similarly, they have a negative effect on growth efficiency of the anodic film. Valota et al. [33] also reported oxygen evolution when anodizing above 40V in glycerol. The presence of oxygen bubbles and reduction in efficiency at high potentials (above 10V in our study) will inform our interpretation of the SEM observations of our specimens, **section 3.4**, and plays an important role in determining the morphology (smooth or ribbed) of the NTs according to the mechanism described in **section 3.5**.

3.4 SEM analysis

Having established that f_g and ε_{NTs} decrease with increasing potential and that fluorine is present in the anodic layer, SEM analysis provides a further insight on the structural changes of the NTs as a result of anodization potential (10-40V) and anodizing time (4-20h). From **Fig. 4a-b**, it is evident that NTs grown at 10V exhibit a smooth surface; they have no ribs on their wall, despite the presence of 2wt% water in the electrolyte. The inset in **Fig. 4b** highlights the porous layer on top of the NTs, which is a remnant of the

initial barrier layer formed at the early stages of anodization [37, 38]; the nano-tubular structure has developed underneath. The influence of anodizing time on the structure becomes clear by comparing **Fig. 4a-b** (4h) and **Fig. 4c-d** (20h). The effect of dissolution is evident in the specimen anodized for 20h; **Fig. 4c** shows the collapse of the NTs, which clump together and is associated with loss of mechanical stability of the NTs due to excessive dissolution of the tube walls. Areas of exposed titanium are also visible where the NTs have detached from the titanium surface. The remnant NTs on the surface lie along the grain boundaries (g.b.) of the titanium substrate and have been highlighted in **Fig. 4c** by dashed lines. In **Fig. 4d** excessive dissolution of the NTs is observed, with some NTs missing a substantial portion of their wall.

Two main conclusions can be drawn from **Fig. 4a-d**. Firstly, due to the presence of a porous layer above the NTs acting as an obstacle for the viscous electrolyte, **Fig 4b**, we suggest the existence of preferential paths for the electrolyte, some of which are correspondingly located at the titanium grain boundaries. If NTs are oriented differently in each titanium grain then larger "V" shaped gaps for the electrolyte could be found at the grain boundaries. As a consequence, dissolution occurs at a faster rate at these locations and NTs are more likely to break away, leaving sections of their structure on the metal substrate to mark the presence of the boundaries. Secondly, dissolution is limited after 4h (**Fig. 4a-b**) but certainly affects the morphology of the NTs at longer anodization times (20h), especially of those that are more exposed to the electrolyte (**Fig. 4d**). Nevertheless the dissolution process alone does not induce the formation of ribs on the nanotube wall, which remain smooth at 10V. In our view, as no significant oxygen evolution is observed at 10V, the smoothness of the NTs is linked to (i) the use of a highly viscous electrolyte [22] and (ii) the absence of bubbles affecting their structure.

Increasing the potential to 20V, **Fig. 5a-d**, changes the morphology of the NTs. In this case all the images in **Fig. 5a-d** correspond to an anodization time of 20h. The growth of the anodic film is affected by oxygen bubbles not only in terms of growth efficiency and f_g, but also in terms of morphology and the NTs grown at 20V exhibit ribs on their side wall, **Fig. 5a-b**. Having established that dissolution alone does not form ribs (i.e. NTs at 10V are smooth), it is clear that the conditions for the formation of ribs are also determined by the applied potential. It appears that ribs generally bridge adjacent NTs, as shown in **Fig.5c** (and inset). Nevertheless there are areas of the anodic film in which the NTs have lost most of the ribs and are smoother in appearance, as in **Fig. 5d** (and inset); a re-shaping which is due to the prolonged effect of dissolution. Hence, ribs are more susceptible than the NTs to chemical attack and dissolution by fluorine ions. This is logical since the surface of the rib is convex and is therefore more active and the surface is more likely to dissolve than if it were flat. On comparing **Fig.5c,** where ribs and bridges are still visible, with **Fig. 5d,** where the NTs appear to have been overdissolved, it is possible to conclude that dissolution occurs to a different extent in different regions of the NTs. This supports the idea of the existence of preferential paths, due to the presence of a porous layer above the NTs, **Fig. 5a** inset.

More details on the origin of ribbed NTs are provided by analysing specimens grown at higher potentials of 30 and 40V. It is still possible to observe an upper porous layer, **Fig. 6a** top left inset, and ribs/bridging, **Fig. 6b**. There are regions where the NT walls have some interesting features. Rather than ribs, the presence of well-defined "oxide rings" can be observed in **Fig. 6b (inset)**. Furthermore regions from which the NTs have been removed, top right inset and main image in **Fig. 6a**, indicate that remnants of the NTs are preferentially left at the grain boundaries (g.b.) of the Ti substrate. A hybrid morphology, where the top region of the NTs are smooth, and a bottom region with ribs is shown in **Fig. 6c** and inset, providing further evidence of the action of the electrolyte and dissolution of fluorine ions which is greater at the top of the nanotube and acts to smooth the nanotube surface. **Fig. 6d** also shows smooth sections of film, likely to be collapsed regions from the top of the NTs.

Similar observations can be drawn from NTs prepared at 40V, **Fig. 7a-f**. The effect of water in the electrolyte is clear by comparing the ribbed structure in **Fig.7a** (2wt% water) with the smooth structure obtained under the same conditions, but with no water added, **Fig.7a** inset. Again, a closer examination of the ribbed structure, **Fig. 7b**, reveals the presence of several oxide rings. These oxide rings are induced by the presence of water and a sufficiently high potential to ensure formation of oxygen bubbles at the anode. It appears as well defined rings are more likely to be preserved at relatively short anodizing time, 4h (i.e. limited dissolution), and ribs are observed wherever the oxide rings have been partially etched/dissolved by the electrolyte, **Fig. 7c**. In other words, ribs are a consequence of the partial dissolution of oxide rings. A

hybrid structure with a bridged bottom and a smooth top on the surface of the NTs is observed in a specimen anodized for 20h, **Fig. 7d-e**, suggesting dissolution is more significant at the top of the anodic structure.
Whereas it seems evident that ribs are generated from partial dissolution of oxide rings, it is not entirely clear why ribs are often bridging together adjacent NTs. A possible explanation is that oxide rings may form an interlocked structure with adjacent rings as a consequence of the plastic flow pushing upward the freshly formed oxide. Partial dissolution of oxide rings leading to ribs bridging adjacent NTs and eventually to fracture of the NTs, is also shown in **Fig. 7f** and inset.
In order to make comparison with the NaF/Glycerol based electrolyte in **Figs 4-7**, we also anodized a specimen at 25V in a NaF/Na_2SO_4/aqueous based solution [39]. As expected the structure is highly disrupted by oxygen bubbles, generated in conjunction with the formation of the NTs, with the presence of several oxide rings, **Fig. 8a**, and ribs bridging the NTs, **Fig. 8b**. It can be argued that if a higher dissolution rate and longer anodizing time contribute to smoothening of the structure in an organic electrolyte, the presence of oxide rings should not be expected in water media, considering the conditions are far more aggressive [39]. However when NTs are formed in water media the anodic structure is highly hydrated [28] and hardens during the anodization process, ejecting some of the excess water [31, 40, 41]. We suggest that once the oxide has hardened, it becomes more resistant to chemical attack by fluorine ions and prevents complete dissolution of oxide rings and ribs.

3.5 Ribs Formation Mechanism

It is clear that several variables contribute to the formation and dissolution of oxide rings and consequently ribs on the NTs. The variables include:
(i) anodizing potential, which above 10V triggers the formation of oxygen bubbles at the anode, a subsequential decresase of the anodic growth factor (f_g) and the growth efficiency (ε_{NTs} **)**, and a change in the morphology of the NTs from a smooth to a ribbed appearance
(ii) anodizing time, with dissolution re-shaping the NTs at longer times as a result of fluorine ions within the anodic film (as confirmed by XPS analysis)
(iii) type of electrolyte (aqueous vs organic) and the presence of water in an organic electrolyte, also affecting the degree of dissolution of the anodic oxide

All these factors can account for the variation in the morphology of the surfaces of the NTs. By combining XPS, SEM and growth efficiency analysis of specimens anodized within the potential range 10-40V we now propose a comprehensive- model to explain the absence or the formation of ribs on anodized TiO_2 NTs.

3.5.1 Stage I (sufficient water and potential leading to oxygen evolution and oxide rings)

The presence of a fluorine rich layer on the outer wall of the NTs and inter-pore/tube regions [23, 24] and the presence of water in the electrolyte accelerate the splitting of the nanopores into NTs [27]. Hence, water is the first requirement for the formation of ribs. In addition, the anodization potential is also an important factor, as can be deduced from the smooth NTs grown at 10V (**Fig. 4a-d**) and ribbed NTs at 20-40V (**Fig. 5-7**). As the anodizing process proceeds, oxide rings are formed on the outer layer of the NTs, **Fig. 9a**. We have previously proposed a growth mechanism in which oxygen evolution contributed to the formation of oxide rings and consequently NTs (stack of rings) in an aqueous system, where oxygen discharged always occurs for conditions used (applied potential ≥ 20V) [31, 40]. From this investigation in an organic media, it can be concluded that oxygen evolution is not necessary for the development of the NTs, as suggested by NTs grown at 10V where oxygen evolution does not occur. Nevertheless, whenever oxygen bubbles are formed, they affect the NT's morphology and induce the formation of oxide rings.

3.5.2 Stage II (partial dissolution of upper part of NTs converting rings into ribs)

As the NTs growth proceeds at the M/MO interface, the initially formed oxide rings are now on the upper part of the NTs and since fluorine ions partially dissolve the structure they are re-shaped from oxide rings to ribs **Fig. 9b**, often bridging adjacent NTs. Considering the higher fluorine concentration on the outer layers and inter-pore/tube regions, oxide rings and ribs are more readily dissolved than the main NTs structure. The rings are present as an artefact of the formation process when the collapsing structure is pushed out by the visco-plastic flow and their formation is aided by gas evolution at the anode. As a consequence of freshly formed oxide being pushed upwards, we suggest that oxide rings contact adjacent rings on the nearby NTs

forming an interlocked bridged structure. As the anodization proceeds, the dissolution of parts of the rings takes place where they are least dense and where electrolyte diffusion is possible. The result is the formation of ribs holding the NTs together.

3.5.3 Stage III (entire NTs array exhibit ribs and bridging)

As the NT growth reaches the limit determined by the conditions (applied potential, electrolyte, time) at the zero growth boundary, chemical dissolution further re-shapes the morphology of the NTs and the oxide rings disappear whereas ribs are visible across the entire length of the NTs, **Fig. 9c**. At this stage dissolution also affects the main NTs structure and thinning of the upper part of the NTs is observed (not in **Fig. 9,** but visible from **Fig.5 c-d**). Eventually the structure collapses as in **Fig. 4c**. The presence of a hybrid structure with a ribbed bottom and smooth top is finally observed when upper ribs are completely removed by dissolution, as depicted in **Fig. 9d**. Considering dissolution is not homogeneous over the entire NTs array, the upper section of the NTs occasionally exhibit non-dissolved rings, as in **Fig. 6b** and **7b**.

The model described here is based on observations made in an organic electrolyte containing 2wt% of water, but it is also valid for aqueous electrolytes. Clearly dissolution phenomena are much more vigorous in water and together with oxygen evolution they significantly disrupt the morphology of the NTs, **Fig. 8a-b**. Partially smooth NTs are therefore not observed in NTs prepared in water, which in contrast always have ribs and bridging. We suggest that ribs are not totally dissolved as they harden by ejecting excess water and become more resistant to attack by fluorine ions.

4. Conclusions

This work has dealt with the formation of ribs on the walls of anodized TiO_2 NTs. A minimum amount of water (few wt%) is necessary to induce the formation of the ribs [21, 22, 33], but the anodization potential also needs to be above a critical value. In our case the critical potential is about 10V, but it is expected to be generally determined by the nature and composition of the electrolyte, water content and fluorine concentration. In summary, the following conclusions can be drawn:

(i) Growth efficiency and anodic growth factor are observed to decrease with increasing anodizing potential. This can be ascribed to an increased ejection of Ti ions into the electrolyte without forming any oxide and also to evolution of oxygen bubbles at higher potentials (20-40V)

(ii) Oxide rings on the outer wall of the NTs are formed when anodizing above 10V (i.e. when the potential is sufficient to cause oxygen bubbles at the anode) for the conditions used in our investigation. At 10V gas bubbles at the anode are not observed and the NTs are smooth. As the oxide rings are more exposed to the electrolyte, have a convex shape and are fluorine rich the rings are more easily dissolved than the main NTs structure. Adjacent oxide rings coming into contact as freshly formed oxide is pushed upwards for effect of the plastic flow may form an interlocked bridged structure

(iii) If the potential is above 10V and oxygen bubbles and oxide rings are formed, partial dissolution of the oxide rings leads to formation of ribbed NTs, with ribs bridging adjacent NTs. Dissolution alone is not a sufficient condition for the formation of rings/ribs as confirmed by the smooth NTs obtained at 10V

(iv) Eventually ribs on the upper part of the NTs are completely dissolved and a hybrid morphology of the anodic film is observed, with a smooth top and a ribbed bottom

(v) The model we proposed applies to both aqueous and organic system and there is strong evidence that rings and ribs occur whenever oxygen bubbles are generated at the anode

Acknowledgements

This work was conducted as part of the Novel-Nano-Templating-Technologies (N2T2) Project (EU, Framework Program 6, contract n. 017481). The authors would like to thank the Royal Academy of Engineers (RAENG) for also supporting this research and Cardiff University for provision of XPS facilities and help with XPS measurements (EPSRC grant EP/F019823/1: Access to Materials Research Equipment-Cardiff XPS). The support from the Slovak Research and Development Agency (projects APVV-0424-10 and APVV-0262-10) is kindly acknowledged.

References

[1] V. Zwilling, M. Aucouturier, E. Darque-Ceretti, Electrochimica Acta, 45 (1999) 921-929.
[2] V. Zwilling, E. Darque-Ceretti, A. Boutry-Forveille, D. David, M.Y. Perrin, M. Aucouturier, Surface and Interface Analysis, 27 (1999) 629-637.
[3] D. Gong, C.G. Grimes, O.K. Varghese, W. Hu, R.S. Singh, Z. Chen, E.C. Dickey, Journal of Materials Research, 16 (2001) 3331-3334.
[4] P. Roy, S. Berger, P. Schmuki, Angew Chem Int Ed Engl, 50 (2011) 2904-2939.
[5] J. Zhao, X. Wang, R. Chen, L. Li, Solid State Communications, 134 (2005) 705-710.
[6] K. Raja, M. Misra, K. Paramguru, Electrochimica Acta, 51 (2005) 154-165.
[7] J.P. O'Sullivan, G.C. Wood, Proceedings of the Royal Society A: Mathematical, Physical and Engineering Sciences, 317 (1970) 511-543.
[8] J.M. Macak, H. Tsuchiya, P. Schmuki, Angew Chem Int Ed Engl, 44 (2005) 2100-2102.
[9] P. Skeldon, G.E. Thompson, S.J. Garcia-Vergara, L. Iglesias-Rubianes, C.E. Blanco-Pinzon, Electrochemical and Solid-State Letters, 9 (2006) B47-B51.
[10] S. Garcia-Vergara, P. Skeldon, G. Thompson, H. Habazaki, Electrochimica Acta, 52 (2006) 681-687.
[11] D.J. LeClere, A. Velota, P. Skeldon, G.E. Thompson, S. Berger, J. Kunze, P. Schmuki, H. Habazaki, S. Nagata, Journal of The Electrochemical Society, 155 (2008) C487-C494.
[12] N. Sato, Electrochimica Acta, 16 (1971) 1683-1692.
[13] M.M. Lohrengel, Materials Science and Engineering R: Reports, 11 (1993) 243-294.
[14] O. Jessensky, F. Müller, U. Gösele, Applied Physics Letters, 72 (1998) 1173-1175.
[15] O. Jessensky, F. Muller, U. Gosele, Journal of The Electrochemical Society, 145 (1998) 3735-3740.
[16] P. Campestrini, G.E. Thompson, P. Skeldon, C.E. Blanco-Pinzon, L. Iglesias-Rubianes, S.J. Garcia-Vergara, Proceedings of the Royal Society A: Mathematical, Physical and Engineering Sciences, 462 (2006) 2345-2358.
[17] J.P.S. Pringle, Electrochimica Acta, 25 (1980) 1423 -1437.
[18] J.S.L. Leach, P. Neufeld, Corrosion Science, 9 (1969) 225-244.
[19] A.C. Crossland, H. Habazaki, K. Shimizu, P. Skeldon, G.E. Thompson, G.C. Wood, X. Zhou, C.J.E. Smith, Corrosion Science, 41 (1999) 1945-1954.
[20] X. Zhou, H. Habazaki, K. Shimizu, P. Skeldon, G.E. Thompson, G.C. Wood, Proceedings of the Royal Society A: Mathematical, Physical and Engineering Sciences, 455 (1999) 385-399.
[21] K.S. Raja, T. Gandhi, M. Misra, Electrochemistry Communications, 9 (2007) 1069-1076.
[22] J.M. Macak, H. Tsuchiya, L. Taveira, S. Aldabergerova, P. Schmuki, Angew Chem Int Ed Engl, 44 (2005) 7463-7465.
[23] S. Berger, S.P. Albu, F. Schmidt-Stein, H. Hildebrand, P. Schmuki, J.S. Hammond, D.F. Paul, S. Reichlmaier, Surface Science, 605 (2011) L57-L60.
[24] A. Jaroenworaluck, D. Regonini, C.R. Bowen, R. Stevens, Applied Surface Science, 256 (2010) 2672-2679.
[25] S. Berger, J. Kunze, P. Schmuki, A.T. Valota, D.J. LeClere, P. Skeldon, G.E. Thompson, Journal of The Electrochemical Society, 157 (2010) C18-C23.
[26] W. Wei, S. Berger, C. Hauser, K. Meyer, M. Yang, P. Schmuki, Electrochemistry Communications, 12 (2010) 1184-1186.
[27] A. Valota, D.J. LeClere, P. Skeldon, M. Curioni, T. Hashimoto, S. Berger, J. Kunze, P. Schmuki, G.E. Thompson, Electrochimica Acta, 54 (2009) 4321-4327.
[28] D. Regonini, A. Jaroenworaluck, R. Stevens, C.R. Bowen, Surface and Interface Analysis, 42 (2010) 139-144.

[29] A.F. Carley, P.R. Chalker, J.C. Riviere, M.W. Roberts, Journal of the Chemical Society, Faraday Transactions 1: Physical Chemistry in Condensed Phases, 83 (1987) 351-370.
[30] M. Textor, C. Sittig, V. Frauchiger, S. Tosatti, D.M. Brunette, Properties and Biological Significance of Natural Oxide Films on Titanium and Its Alloys, in: Titanium in Medicine: Material Science, Surface Science, Engineering, Biological Responses and Medical Applications, Springer Verlag, Heidelberg and Berlin
2001, pp. 171-230.
[31] A. Jaroenworaluck, D. Regonini, C.R. Bowen, R. Stevens, Journal of Materials Research, 23 (2008) 2116-2124.
[32] D. Regonini, A. Satka, D. Allsopp, A. Jaroenworaluck, R. Stevens, C.R. Bowen, Journal of Nanoscience and Nanotechnology, 9 (2009) 4410-4416.
[33] A. Valota, M. Curioni, D.J. Leclere, P. Skeldon, P. Falaras, G.E. Thompson, Journal of The Electrochemical Society, 157 (2010) K243-K247.
[34] K. Yasuda, J.M. Macak, S. Berger, A. Ghicov, P. Schmuki, Journal of The Electrochemical Society, 154 (2007) C472-C478.
[35] H. Habazaki, M. Uozumi, H. Konno, K. Shimizu, S. Nagata, K. Takayama, Y. Oda, P. Skeldon, G.E. Thompson, Journal of The Electrochemical Society, 152 (2005) B263-B270.
[36] K. Zhu, N.R. Neale, A. Miedaner, A.J. Frank, Nano Letters, 7 (2006) 69-74.
[37] M. Paulose, K. Shankar, S. Yoriya, H.E. Prakasam, O.K. Varghese, G.K. Mor, T.A. Latempa, A. Fitzgerald, C.G. Grimes, Journal of Physical Chemistry B, 110 (2006) 16179-16184.
[38] D. Kim, A. Ghicov, P. Schmuki, Electrochemistry Communications, 10 (2008) 1835-1838.
[39] D. Regonini, C.R. Bowen, R. Stevens, D. Allsopp, A. Jaroenworaluck, Physica Status Solidi (a), 204 (2007) 1814-1819.
[40] A. Jaroenworaluck, D. Regonini, C.R. Bowen, R. Stevens, D. Allsopp, Journal of Materials Science, 42 (2007) 6729-6734.
[41] T. Ohtsuka, T. Otsuki, Corrosion Science, 45 (2003) 1793-1801.

Figures, Tables and Captions

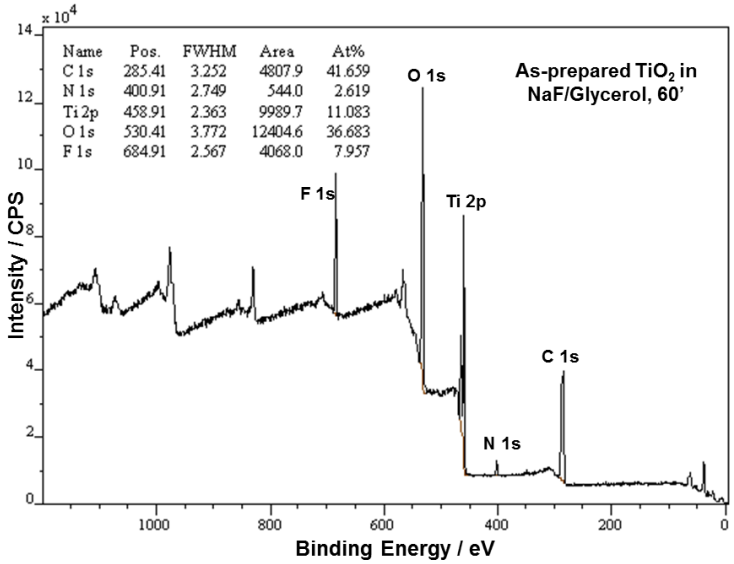

Figure 1. XPS spectra of as-prepared anodized TiO_2 NTs grown in NaF/glycerol for 60minutes. Main impurities are fluorine and carbon species.

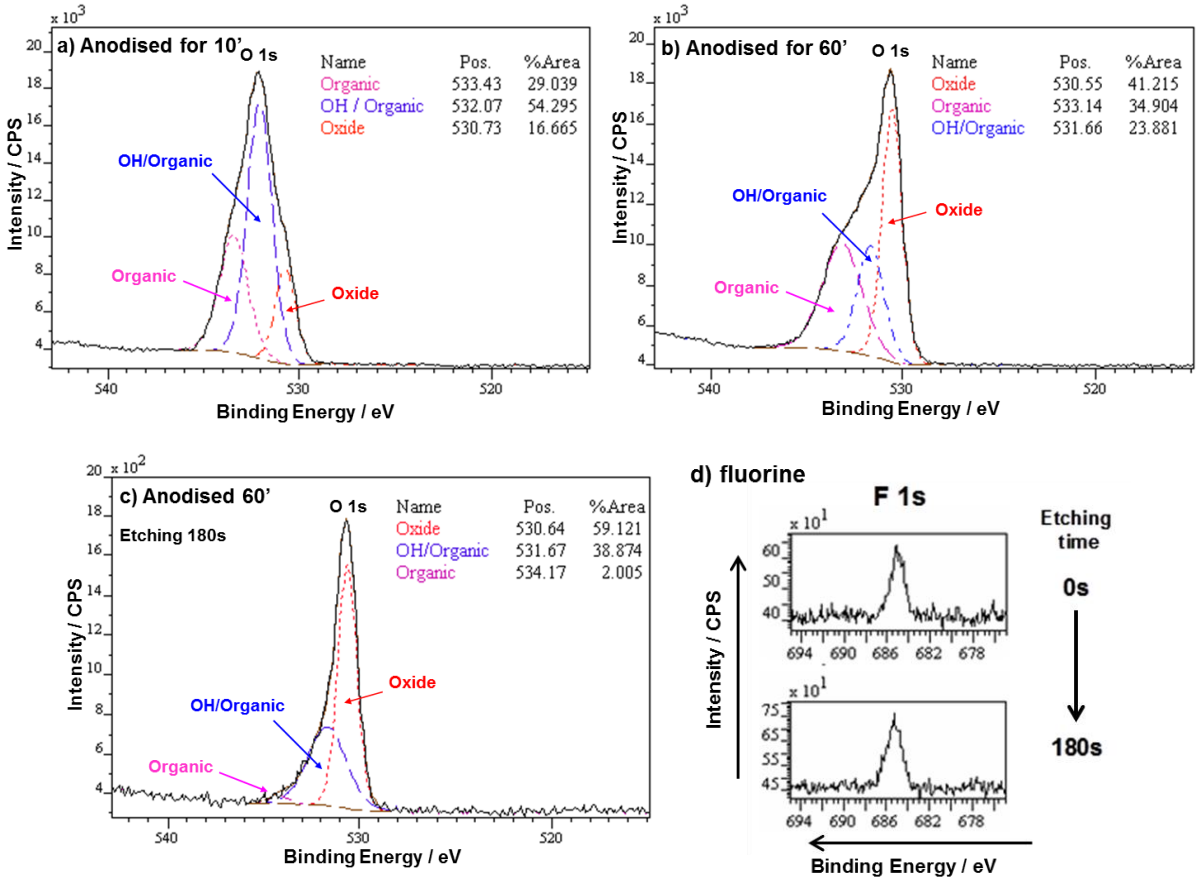

Figure 2a-d. Evolution of the oxygen peak with time when anodising Ti in NaF/Glycerol (**a-c**): the organic components dominate at the early stages, 10min (**a**), while the oxide peak becomes much more intense after 60min (**b**). After removing a few atomic layers by etching, the true composition of the film emerges, with the oxide representing 60% of the total oxygen signal (**c**). Depth profiling also reveals fluorine contamination to be generally constant (on the macroscale) across the anodic film (**d**).

Potential / *V*	d_i / nm	w / nm	d_e / nm	f_g / nm V^{-1}
10	*19.5 ± 1.8*	*10.7 ± 1.0*	*40.9 ± 2.1*	*2.0 ± 0.1*
20	*33.1 ± 6.5*	*13.9 ± 1.3*	*61.1 ± 6.6*	*1.5 ± 0.1*
30	*62.9 ± 4.5*	*18.6 ± 2.1*	*100.2 ± 5.0*	*1.7 ± 0.1*
40	*75.9 ± 2.8*	*24.1 ± 2.2*	*124.2 ± 3.6*	*1.6 ± 0.1*

Table 1. Internal (d_i) and external (d_e) diameters, wall thickness **(**w**)** and anodic growth factor (f_g) calculated for the NTs grown over the potential range 10-40V.

Potential / *V*	Q / A sec	$T_{id.}$ at 4h / nm	T_{real} at 4h / nm	P	ε_{NTs} / %
10	$4.09 \cdot 10^{-5}$	*492*	*~500*	*0.30*	*71 (>100)*
20	$9.68 \cdot 10^{-5}$	*1164*	*~1000*	*0.36*	*55 (86)*
30	$1.18 \cdot 10^{-4}$	*1418*	*~1500*	*0.45*	*58 (>100)*
40	$3.38 \cdot 10^{-4}$	*4060*	*~1000*	*0.43*	*14 (25)*

Table 2. Average charge per minute (Q**)**, ideal ($T_{id.}$**)** and real (T_{real}**)** thicknesses of NTs at 4h, porosity (P) and growth efficiency (ε_{NTs}**)** of the anodizing process over the range 10-40V (efficiency values in brackets do not account for porosity generated by flow mechanism and are therefore an overestimate).

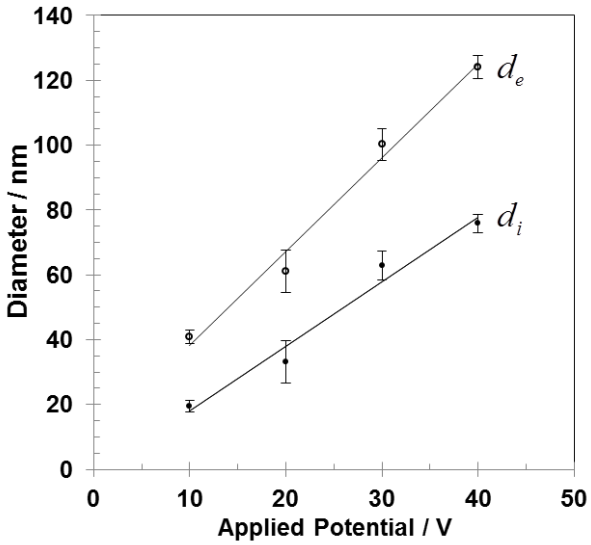

Figure 3. Linear dependence from potential observed for the inner and outer diameter of NTs grown in NaF/Glycerol over the range 10-40V.

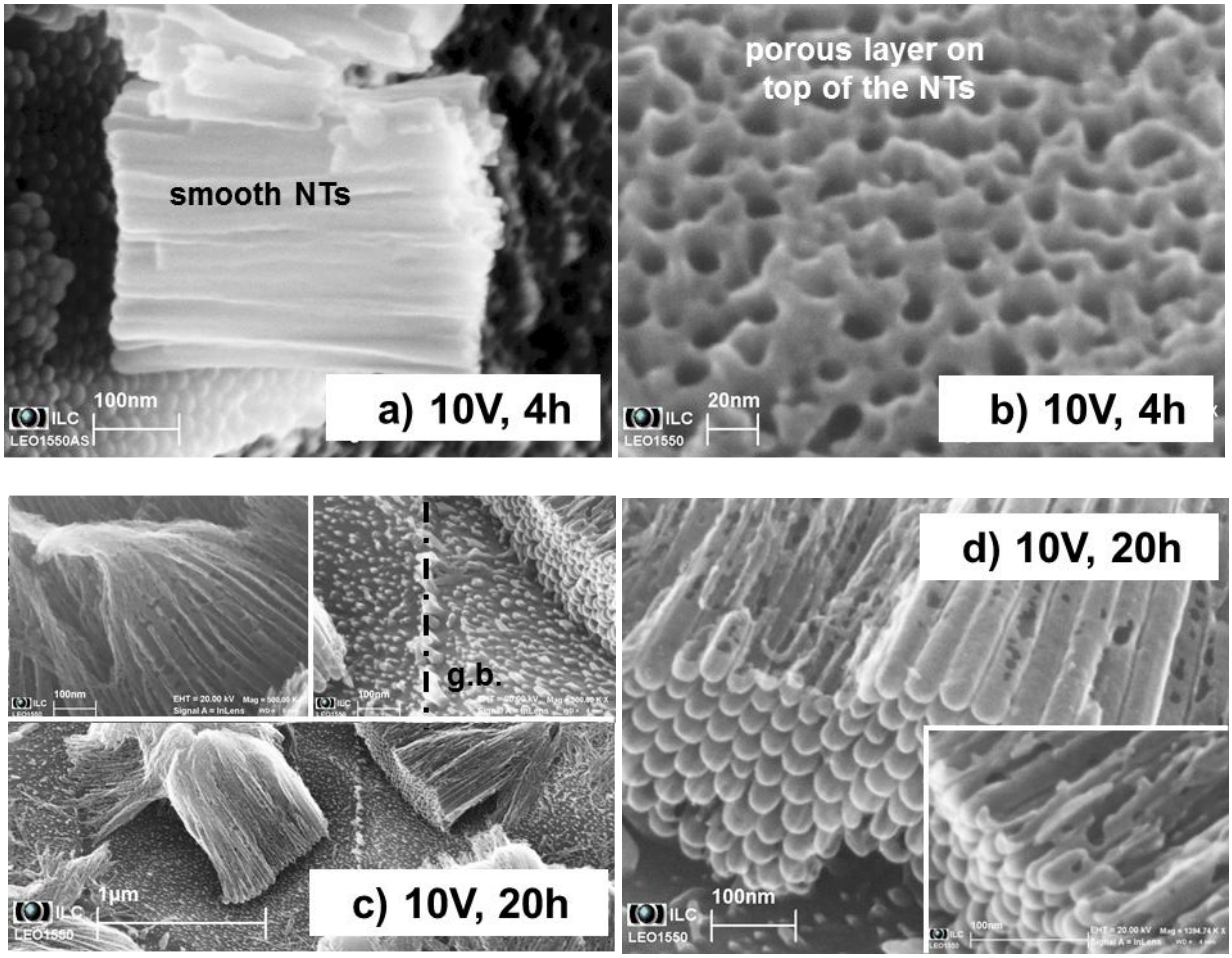

Figure 4a-d. SEM images of the NTs grown at 10V for 4h (**a-b**) and 20h (**c-d**). The NTs are smooth and dissolution affects their structure over extended time (20h), eventually leading to the collapse of the tubes (**c**) and removal of wall sections of the NTs when exposed to the electrolyte for long times (**d**).

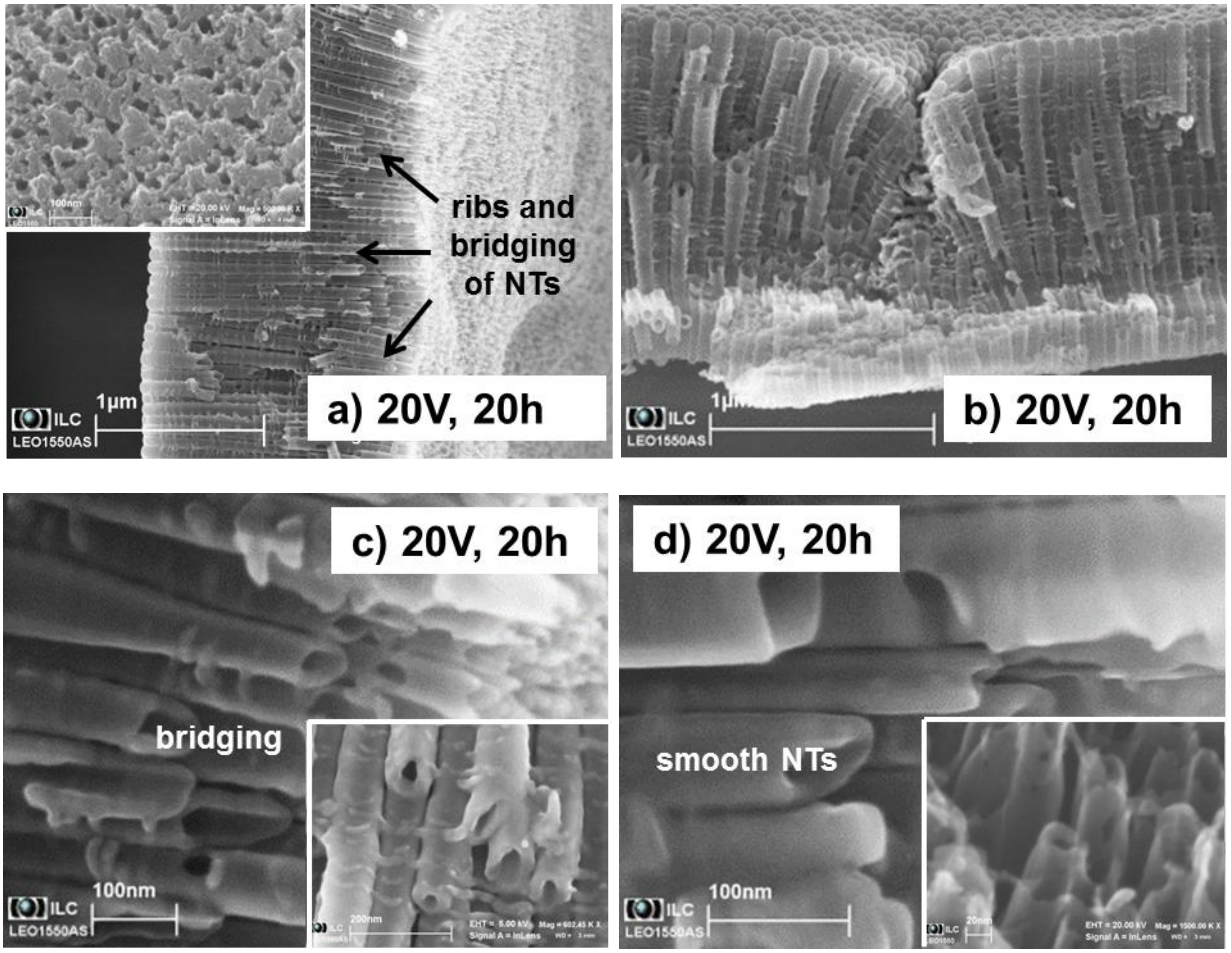

Figure 5a-d SEM images of the NTs grown at 20V for 20h (**a-d**). The NTs have ribs (**a**, **b**) which in some cases bridge adjacent NTs (**b,c**). Areas where the action of fluorine ions has been more aggressive (higher dissolution) exhibit an almost smooth morphology (**d)**.

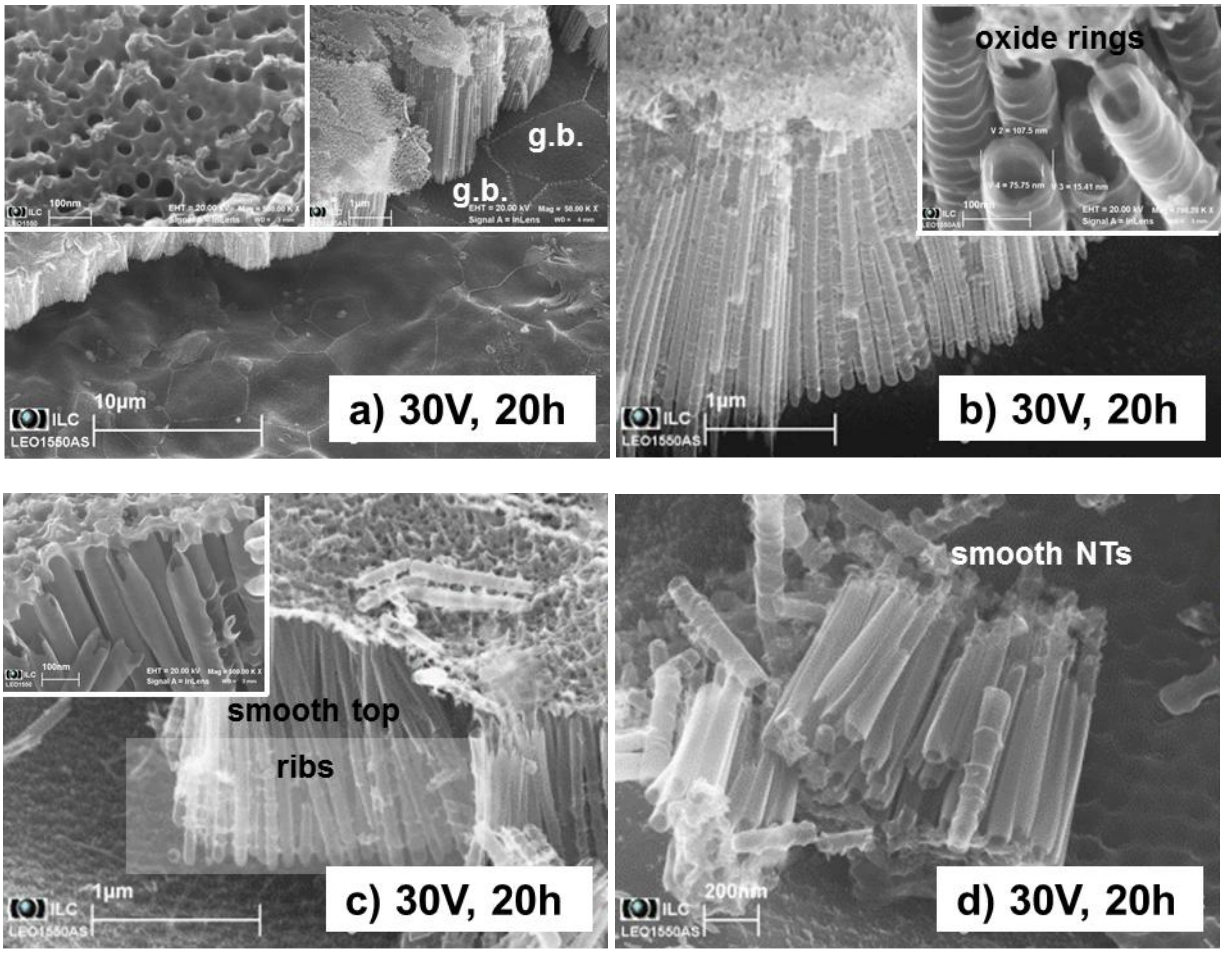

Figure 6a-d. SEM images of the NTs grown at 30V for 20h (**a-d**). A porous layer is located above the NTs, the remains of detached NTs delineating the grain boundaries (g.b.) of the Ti substrate (**a**). Again the presence of ribs/bridging and well defined "oxide rings" (**b**) is clear. A hybrid morphology, smooth top and ribs at the bottom as a result of fluorine dissolving the oxide preferentially from the top towards the bottom (c). Details of a smooth section of collapsed NTs (**d)**.

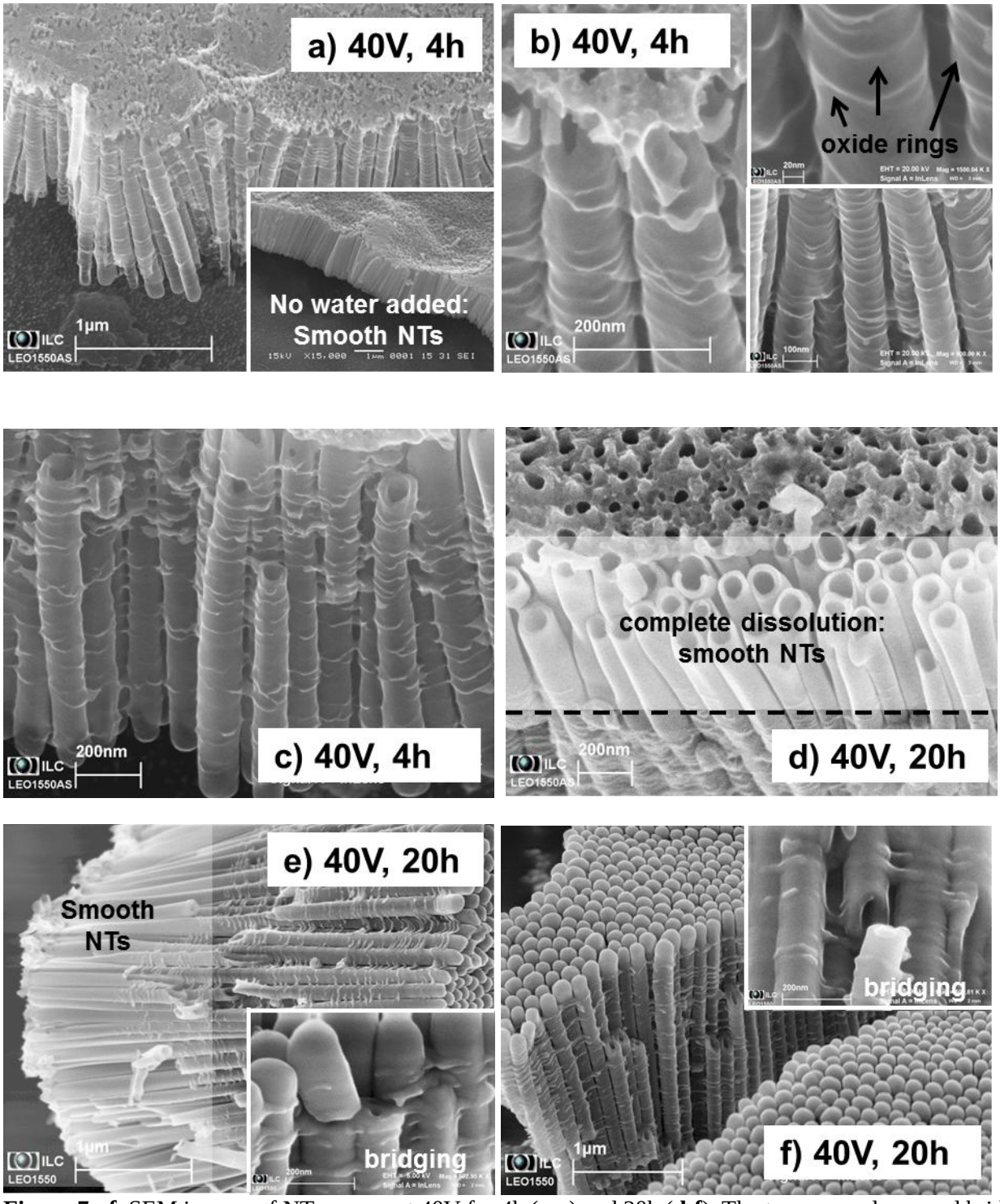

Figure 7a-f. SEM images of NTs grown at 40V for 4h (**a-c**) and 20h (**d-f**). The top porous layer and bridging of NTs are clearly observed, with the inset showing smooth NTs in "water-free" electrolyte (**a**). The presence of well-defined oxide rings on areas where dissolution has been minimal (**b**) and coalescence of rings (bridging) (**c**). Hybrid morphology (smooth top and ribs at bottom) become visible at longer times, 20h (**d-e**); details of the bridging and breaking of NTs section (**e-f**).

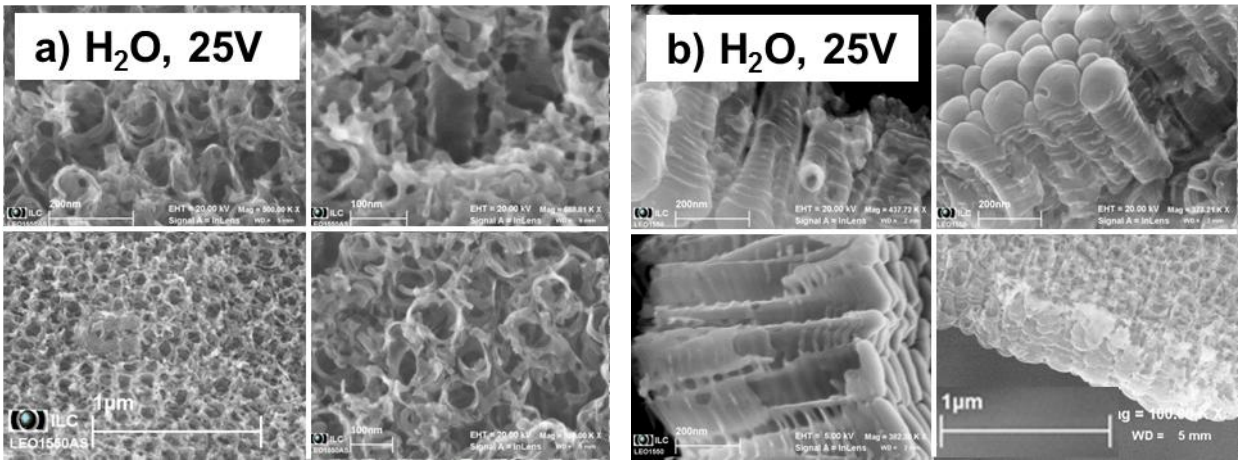

Figure 8a-b. SEM images of the NTs grown at 25V in a NaF/Na_2SO_4 aqueous electrolyte (**a-b**). Top-view images highlight the presence of "oxide rings", the majority are partially destroyed as a consequence of the relatively chemical dissolution observed in water in comparison with organic media (**a**). A transverse section provides more details on the presence of ribs and bridges among adjacent NTs (**b**).

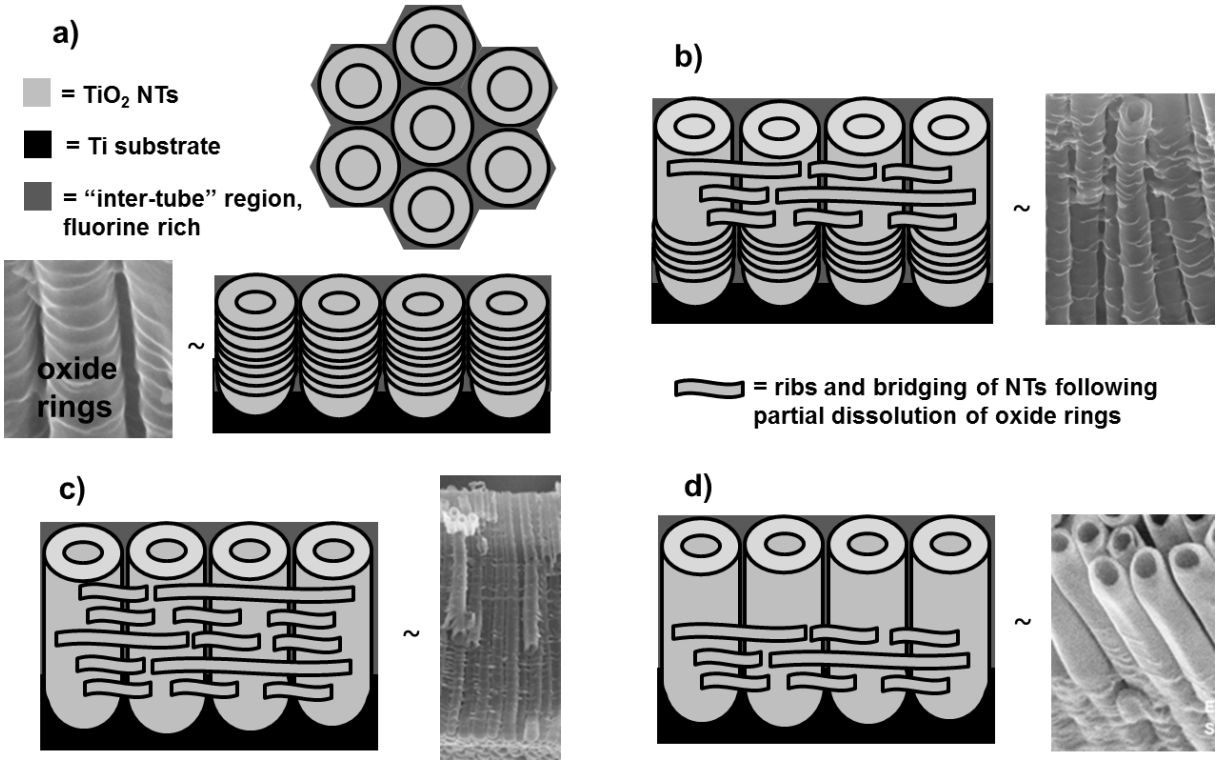

Figure 9a-d. Schematic of the mechanism of formation of ribs on anodized TiO_2 NTs. In the presence of a critical amount of water (few %) and a sufficient potential, the NTs forms with an outer layer characterised by "oxide rings" (**a**). As the anodization proceeds at the M/MO interface, the upper part of the NTs is more exposed to dissolution and the rings converts into ribs loosely attached to the NTs structure and bridging adjacent NTs (**b**). Eventually the entire NTs array exhibit ribs and bridging (**c**), although at longer time completely dissolution of the ribs on the upper part of the NTs leads to hybrid structure characterised by a smooth top and a ribbed bottom (**d**).

***Response to Reviewers**

Minor Revision to Manuscript following reviewers and editor recommendations/guidelines

Previous Version	**Revised/Changed to:**
The objective of this paper is to examine in detail the mechanism of formation of ribs and propose a holistic model which holds true for both aqueous and organic electrolytes.	The objective of this paper is to examine in detail the mechanism of formation of ribs and propose a model which holds true for both aqueous and organic electrolytes.
Dissolution, although secondary, may thin away the oxide layer or detach of a section of the film and finally there may be "electronic" side reactions occurring at the anode, such as oxygen or even hydrogen evolution, the latter caused by corrosion of the Ti substrate [37]. In our specimens corrosion pits are absent whereas over the range 20-40V we have observed oxygen gas evolving at the anode.	Dissolution, although secondary, may thin away the oxide layer or detach of a section of the film and finally there may be "electronic" side reactions occurring at the anode such as oxygen evolution, which we observe for specimens anodized over the range 20-40V.
Terms: Voltage	Replaced either by applied potential or potential
Graphs and table headings	Adapted to Electrochimica Acta format wherever possible